Hindawi
Complexity
Volume 2021, Article ID 8848904, 12 pages
https://doi.org/10.1155/2021/8848904

Research Article

A Linear Parameter Varying Control Approach for DC/DC Converters in All-Electric Boats

Soroush Azizi,[1] **Mohammad Hassan Asemani**,[1] **Navid Vafamand**,[1] **Saleh Mobayen**,[2,3] **and Mohammad Hassan Khooban**[4]

[1]*Department of Electrical and Computer Engineering, Shiraz University, Shiraz, Iran*
[2]*Future Technology Research Center, National Yunlin University of Science and Technology, Douliu, Yunlin, Taiwan*
[3]*Department of Electrical Engineering, University of Zanjan, Zanjan, Iran*
[4]*Department of Engineering, Aarhus University, Aarhus, Denmark*

Correspondence should be addressed to Mohammad Hassan Asemani; asemani@shirazu.ac.ir and Saleh Mobayen; mobayen@znu.ac.ir

Received 28 September 2020; Revised 11 January 2021; Accepted 9 February 2021; Published 24 February 2021

Academic Editor: Carlos Aguilar-Ibanez

Utilization of renewable energies in association with energy storage is increased in different applications such as electrical vehicles (EVs), electric boats (EBs), and smart grids. A robust controller strategy plays a significant role to optimally utilize the energy resources available in a power system. In this paper, a suitable controller for the energy resources of an EB which consists of a 5 kW solar power plant, 5 kW fuel cell, and 2 kW battery package is designed based on the linear parameter varying (LPV) controller design approach. Initially, all component dynamics are augmented, and by exploiting the sector-nonlinearity approach, the LPV representation is derived. Then, the LPV control method determines the suitable gains of the states' feedbacks to provide the required pulse commands of the boost converters of the energy resources to regulate the DC-link voltage and supply the power of EB loads. Comparing with the state-of-the-art nonlinear control methods, the developed control approach assures the stability of the overall system, as it considers all component dynamics in the design procedure. The real-time simulation results demonstrate the performance of the designed controller in the creation of a constant DC-link voltage.

1. Introduction

The popularity of renewable energies results from the reduction of reachable fossil fuels and an increase in their cost. Literature has widely studied the application of renewable energies in the propulsion system of electric vehicles (EVs) [1–3] and electric boats (EBs) [4]. The DC-DC power converters and their control systems have prominent duties in the energy conversion of such vehicles. For instance, low voltage battery packages need step-up converters to provide the required voltage for the DC-link of these vehicles [5]. For this reason, while the conventional boost converters are used as an interface circuit in the structure of the EVs and EBs propulsion system, a suitable robust controller is required to guarantee the correct operation of the converters [6–11].

The mathematical and black-box analyses of a power converter are two different approaches to design the controllers of the power converters. In comparison with the black-box analysis, the mathematical analysis of the systems results in a more reliable response in a wide range of operating points. State-space averaging, discrete averaged model, G-parameter modeling, component connection model, describing the function, and linear parameter varying (LPV) are the most used mathematical analysis in the controller designs. In [12], a state-space averaging model has been proposed for a bidirectional converter. For DC-DC converters with pulsating output current, such as boost converters, the use of leading-edge or trailing-edge pulse-width modulation (PWM) brings about distinctly different behavior [13]. This phenomenon cannot be captured by the conventional averaged model but is predicted with a discrete-time model. The results of the proposed approximate discrete-

time model in [14] demonstrate the successful performance of the control system of a boost converter. Although the discrete averaged model works well for a single bidirectional converter, the extraction of the averaged model for a system for more than two converters is a challenging procedure. In fact, it is hard to provide an accurate discrete-time averaged model to use two different converters while supplying a load.

G-parameter model and component connection model are two outstanding procedures while various power converters work in a system. However, the G-parameter just considers small signals of the model which limit its application for different operating modes. Also, the component connection is a mapping technique that can be used in the stability analysis of a system. Therefore, these techniques cannot work properly in the controller design of converters in EBs or smart grids while different variables can affect their operating modes. Moreover, the described function technique is able to consider single nonlinearity and cannot design a robust controller in the presence of various nonlinearity or uncertainties. It has been proven that the LPV can be employed in the design of large-scale hybrid systems controllers. The LPV technique benefits from its ability in the design of a robust controller for large signal analysis in the presence of a wide range of uncertainties. In [15, 16] and [17], the LPV is used to design a high-performance controller for the pitch angle of wind turbines [18, 19]. Besides, the LPV has been used to design a controller for a single boost converter for a photovoltaic (PV) array which supplies load in [20].

In this paper, a comprehensive controller for boost power converters of an electric boat propulsion system is designed based on the polytopic-LPV technique. The considered EB is supplied by a 5 kW solar array, 5 kW fuel cell package, and 2 kW batteries. The gate commands of such a hybrid system are determined by the designed controller to create a stiff DC-link voltage in different solar irradiations and loads. Initially, the topology of the investigated system is described. Then, the polytopic-LPV controller design procedure for the system is designed such that the exponential stability of the overall system is assured. The proposed approach has some advantages over state-of-the-art methods, including the following: (1) it considers the available information of all components in the design procedure compared to [21–23]. Therefore, the overall closed-loop stability is guaranteed theoretically through the Lyapunov stability theory [24–29]. (2) The design procedure of the proposed controller is simple and systematic compared to the other method [30, 31]. Additionally, the controller gains can be computed by using the numerical convex optimization linear matrix inequality (LMI) techniques. (3) The proposed controller is more robust against system parameter variations and uncertainties compared to [32, 33]. Finally, a real-time simulation study is executed on the DC MG power system to examine the performance of the proposed controller.

The rest of this paper is as follows: in Section 2, the power sources and their dynamics in the overall EB system are discussed. In Section 3, the LPV approach to model the nonlinear dynamics of the propulsion power system and to design the control is presented. In Section 4, simulation results are provided, and Section 5 ends the paper by giving some concluding remarks and future perspectives.

2. The Power Propulsion System of the EB

Figure 1 shows the power propulsion system of the EB investigated in this paper. It is obvious that the propulsion system, consisting of the photovoltaic array, fuel cell, and battery package, aims to supply the 10 kw load available on their common DC-link. The boost converters which are used as the interface circuit of these power sources must be controlled properly to provide the required DC-link voltage. In this section, the characteristics of each power source and its state-space model are studied.

2.1. Solar Power Plant. A 5 kw solar power plant with the maximum voltage and current of 200 V and 25 A is one of the energy resources of the EB propulsion system. As it is shown in Figure 2, the output of the PV array is connected to a DC-DC boost converter which supplies the DC-link capacitor. The dynamics of the PV cell linked to the boost converter is as follows [34]:

$$\begin{cases} \dfrac{V_{\mathrm{PV}}}{\mathrm{d}t} = \dfrac{I_{\mathrm{PV}} - I_{L_{\mathrm{PV}}}}{C_{\mathrm{PV}}}, \\ \dfrac{\mathrm{d}I_{L_{\mathrm{PV}}}}{\mathrm{d}t} = \dfrac{V_{\mathrm{PV}} - \left(1 - D_p\right)V_{\mathrm{DC}}}{L_{\mathrm{PV}}}, \end{cases} \tag{1}$$

where I_{PV}, V_{PV}, V_{DC}, and D_P are the PV array current, PV array voltage, DC-link voltage, and duty cycle of the boost converter switch, respectively. Also, L_{PV} and C_{PV} show the inductance and input capacitor of the boost converter available in the interface circuit of the solar power plant. The boost converter switching control plays a significant role in the determination of the output voltage of the solar array to generate the maximum power. Therefore, a suitable controller must be designed to achieve the maximum power from the PV array in different solar irradiations. Also, the boost converter is to provide the required DC-link voltage. Hence, the boost converter state-space model is extracted to use this model during the controller design procedure. The converter state-space equation is written by (2) which is used in the controller design procedure, where U_1 is the command signal for the PV array boost converter (Q_1).

As it is expected, the effect of load shown by (R_L) appears in the DC-link voltage equation:

$$\begin{cases} \dfrac{dV_{PV}}{dt} = \dfrac{I_{PV}}{C_{PV}} - \dfrac{I_{L_{PV}}}{C_{PV}} = \dfrac{I_{PV}}{C_{PV}V_{PV}}V_{PV} - \dfrac{I_{L_{PV}}}{C_{PV}}, \\ \dfrac{dI_{L_{PV}}}{dt} = \dfrac{V_{PPVV}}{L_{PV}} - \dfrac{V_{DC}U_1}{L_{PV}}, \\ \dfrac{dV_{DC}}{dT} = \dfrac{I_{PV}U_1}{C_{DC}} - \dfrac{V_{DC}}{C_{DC}R_L}. \end{cases} \tag{2}$$

2.2. Fuel Cell. If the 5 kw fuel cell package is replaced with the PV array represented in Figure 2, the second energy resource of the system can be connected to the DC-link capacitor. The inductance of the fuel cell boost converter is equal to L_{PV}, because of the same power rating and switching frequency of both converters. Also, the DC voltage at the output of the fuel cell remains constant while it supplies the load. Thus, as it is shown in Figure 3, the boost converter of the fuel cell does not require any capacitor in its model. The state-space equation of the fuel cell, working in parallel with the solar array, can be written as follows:

$$\begin{cases} \dfrac{dI_{L_F}}{dt} = \dfrac{V_F}{L_F} - \dfrac{V_{DC}U_2}{L_F} = \dfrac{V_F}{L_F I_F}I_F - \dfrac{V_{DC}U_2}{L_F}, \\ \dfrac{dV_{DC}}{dt} = \dfrac{I_{L_F}U_2}{C_{DC}} - \dfrac{V_{DC}}{C_{DC}R_L}. \end{cases} \tag{3}$$

where L_F and U_2 represent the boost converter inductance and duty cycle of the switching for the boost converter of the fuel cell. Moreover, the fuel cell output current and voltage are shown by I_F and V_F, respectively.

2.3. Energy Storage. A 2 kw battery package is investigated to work in parallel with the introduced energy sources to regulate the DC-link voltage of the system when two other sources cannot supply the load. In addition, when the solar power plant generates a higher energy level than the load, the energy storage starts to store the extra generated energy. Therefore, a bidirectional converter is required for the energy storage to balance the energy level on the DC-link. The lead-acid battery can be simply modeled by the following equation:

$$V_B = V_G - R_s I_B, \tag{4}$$

where V_G is the plate voltage level of the battery package and R_S is the equivalent series resistance of the battery. Therefore, the output voltage of the battery shown with V_B depends on the output current of the battery. The dynamics of the bidirectional converter presented in Figure 4 is as follows:

$$\begin{cases} \dfrac{dI_{L_B}}{dt} = \dfrac{V_B - D_B V_{DC}}{L_B}, \\ \dfrac{dV_B}{dt} = \dfrac{I_B - I_{L_B}}{C_B}, \end{cases} \tag{5}$$

where L_B and C_B show the bidirectional converter inductance values and D_B is the duty cycle of the Q_3 shown in Figure 4. The state-space model of the energy storage, written in (6), connected to the same DC-link with two other introduced resources is required to design the controller based on the LPV approach:

$$\begin{cases} \dfrac{dV_B}{dt} = \dfrac{I_B}{C_B} - \dfrac{I_{L_B}}{C_B} = \dfrac{I_B}{C_B V_B}V_B - \dfrac{I_{L_B}}{C_B}, \\ \dfrac{dI_{L_B}}{dt} = \dfrac{V_B}{L_B} - \dfrac{V_{DC}U_3}{L_B}, \\ \dfrac{dV_{DC}}{dt} = \dfrac{I_{L_B}U_3}{C_{DC}} - \dfrac{V_{DC}}{C_{DC}R_L}, \end{cases} \tag{6}$$

where I_B and V_B are the current and voltage of the battery package, respectively. Also, U_3 represents the Q_3 command signal, and the bidirectional converter inductor current is shown by I_B.

2.4. Overall State-Space Model. Based on the nonlinear dynamics of the solar power plant, fuel cell, and their boost converters and the bidirectional converter of the energy storage system, the following overall state-space representation is obtained:

$$\dot{x}(t) = A(t)x(t) + B(t)u(t), \tag{7}$$

where $x(t) = [V_{PV}, I_{L_{PV}}, I_{L_F}, V_B, I_{L_B}, V_{DC}, Z]^T$ is the state vector and $A(t)$ and $B(t)$ matrices are

$$A(t)=\begin{bmatrix} \frac{I_{\mathrm{PV}}}{C_{Pv}V_{\mathrm{PV}}} & \frac{-1}{C_{\mathrm{PV}}} & 0 & 0 & 0 & 0 & 0 \\ \frac{1}{L_{\mathrm{PV}}} & 0 & 0 & 0 & 0 & 0 & 0 \\ 0 & 0 & \frac{V_F}{L_F I_F} & 0 & 0 & 0 & 0 \\ 0 & 0 & 0 & \frac{I_B}{C_B V_B} & \frac{-1}{C_B} & 0 & 0 \\ 0 & 0 & 0 & \frac{1}{L_B} & 0 & 0 & 0 \\ 0 & 0 & 0 & 0 & 0 & \frac{-1}{R_L C_{\mathrm{DC}}} & 0 \\ 0 & 0 & 0 & 0 & 0 & -1 & 0 \end{bmatrix}, \quad (8)$$

$$B(t)=\begin{bmatrix} 0 & -\frac{V_{\mathrm{DC}}}{L_{\mathrm{PV}}} & 0 & 0 & 0 & \frac{I_{L_{\mathrm{PV}}}}{C_{\mathrm{DC}}} & 0 \\ 0 & 0 & -\frac{V_{\mathrm{DC}}}{L_F} & 0 & 0 & \frac{I_{L_F}}{C_{\mathrm{DC}}} & 0 \\ 0 & 0 & 0 & 0 & -\frac{V_{\mathrm{DC}}}{L_B} & \frac{I_{L_B}}{C_{\mathrm{DC}}} & 0 \end{bmatrix}^T.$$

As can be seen in (7), the overall dynamics are nonlinear and time-varying due to the fact that the matrices $A(t)$ and $B(t)$ contain system states and time-varying parameters of the nonlinear power elements. Additionally, the duty cycle control inputs in $u(t)$ are amplitude bounded. These issues make the controller design procedure a hard task. To design a controller that theoretically guarantees closed-loop stability, the polytopic-LPV representation is utilized in the following section.

3. Polytopic-LPV Technique

The polytopic-LPV method provides a systematic and straightforward procedure to analyze the stability and design of a stabilizing controller for a nonlinear system. To perform this, initially, the nonlinear system is rewritten by an equivalent polytopic-LPV model. Then, the gains of a polytopic-LPV control law are chosen such that the closed-loop system assures the Lyapunov stability [35].

3.1. Polytopic-LPV Model of DC MG. In order to achieve the objectives of the microgrid, the polytopic-LPV control approach is utilized in this paper. In the state-space model, there are some time-varying terms $(I_{pv}/C_{pv}Vpv)$, $(V_F/L_F I_F)$, and $(I_B/C_B V_B)$ in the matrix A and state variables $I_{L_{\mathrm{PV}}}$, I_{L_B}, I_{L_F}, and V_{DC} in the matrix B. Let

$$\theta=\begin{bmatrix}\theta_1 & \theta_2 & \dots & \theta_7\end{bmatrix}^T=\begin{bmatrix}\frac{I_{\mathrm{PV}}}{C_{\mathrm{PV}}V_{\mathrm{PV}}} & \frac{V_F}{L_F I_F} & \frac{I_B}{C_B V_B} & V_{\mathrm{DC}} & I_{L_{\mathrm{PV}}} & I_{L_F} & I_{L_B}\end{bmatrix}^T \quad (9)$$

to be the vector of varying parameters, where each parameter is bounded in a set, $\theta\varepsilon[\underline{\theta},\overline{\theta}]$, with $\overline{\theta}$ and $\underline{\theta}$ as the upper and lower limits, respectively. The values of vector θ are contained in a polytopic domain with 2^7 vertices. Finally, by applying the so-called sector nonlinearity [36, 37], the following polytopic-LPV system is obtained:

$$\begin{cases} \dot{x}(t)=\sum_{i=1}^{128}\rho_i(\theta)\{A_i x(t)+B_i v(t)\}, \\ y(t)=Cx(t), \end{cases} \quad (10)$$

where $v(t)=\mathrm{sat}(u(t))=[\mathrm{sat}(u_1(t)),\dots,\mathrm{sat}(u_3(t))]^T$ and

$$\mathrm{sat}(u_i(t))=\begin{cases} 1, & u_i(t)\geq 1, \\ u_i(t), & \text{for } 1<u_i(t)<1, \\ -1, & u_i(t)\leq -1. \end{cases} \quad (11)$$

Note that, to design the pulse-width modulation (PWM) signal for the converters, it is necessary that the duty cycles u_i for $i=1,2,3$ are bounded by ± 1. Thereby, the lower and upper bounds in (10) are -1 and $+1$, respectively. The goal is to design the control input vector $u(t)$ such that the V_{PV} tracks the voltage of the $V_{\mathrm{PV-ref}}$ and the DC bus voltage converges to V_{DC}^*. The reference value of the DC bus voltage is mainly constant. However, the maximum power point voltage reference must be chosen accordingly.

3.2. LPV Controller Design. In order to achieve the objectives of the microgrid, the polytopic-LPV control approach is utilized in this paper:

$$u(t)=\sum_{i=1}^{128}\rho_i(\theta)F_i x(t), \quad (12)$$

where F_i for $i=1,\dots,128$ are the controller gains, which should be obtained to assure the closed-loop stability and convergence of the states V_{PV} and V_{DC} to their references. By

adding the null term $\sum_{i=1}^{r} h_i(z(t))B_i(1+\varepsilon/2)(u(t)-u(t))$ with $0<\varepsilon<1$ to (10), one has

$$\begin{aligned}\dot{x}(t) &= \sum_{i=1}^{128}\rho_i(\theta)\left\{A_i x(t) + B_i\frac{1+\varepsilon}{2}u(t) + B_i\left(v(t) - \frac{1+\varepsilon}{2}u(t)\right)\right\}\\ &= \sum_{i=1}^{128}\rho_i(\theta)\left\{A_i x(t) + B_i\frac{1+\varepsilon}{2}u(t) + B_i r(t)\right\},\end{aligned} \tag{13}$$

where $r(t) = v(t) - (1+\varepsilon/2)u(t)$. The closed-loop system is obtained as

$$\dot{x}(t) = \sum_{i=1}^{128}\sum_{j=1}^{128}\rho_i(\theta)\rho_j(\theta)\left\{\left(A_i + \frac{1+\varepsilon}{2}B_i F_j\right)x(t) + B_i r(t)\right\}. \tag{14}$$

Lemma 1 (see [38]). *For the saturation constraint defined by (11), as long as $|u(t)| < (1/\varepsilon)$ with $0<\varepsilon\le 1$, one has*

$$r^T(t)r(t) \le \left(\frac{1-\varepsilon}{2}\right)^2 u^T(t)u(t), \tag{15}$$

which is shown in Figure 5.

Lemma 2 (S-procedure) (see [39]). *Consider that the conditions*

$$\zeta^T T_0 \zeta \ge 0, \tag{16}$$

where $\zeta \ne 0$ and satisfies the constraints

$$\zeta^T T_i \zeta \ge 0, \quad \text{for } i = 1,\ldots,p. \tag{17}$$

Then, condition (16) subject to constraint (17) results in

$$T_0 - \sum_{i=1}^{p}\tau_i T_i \ge 0, \tag{18}$$

where τ_i for $i = 1,\ldots,p$ are arbitrary nonnegative scalars.

Lemma 3 (see [40]). *ie time-varying parameter-dependent constraint $\sum_{i=1}^{q}\sum_{j=1}^{q}\rho_i(\theta)\rho_j(\theta)x^T\Gamma_{ij}x(t) < 0$ is implied by the following time-varying parameter independent conditions:*

$$\begin{cases}\Gamma_{ii} < 0, & \text{for } i = 1,\ldots,q,\\ \Gamma_{ij} + \Gamma_{ji} < 0, & \text{for } i < j \text{ and } j = 1,\ldots,q.\end{cases} \tag{19}$$

Lemma 1 is essential to eliminate the time-varying parameters $\rho_i(\theta)$ and the state vector x in the controller design conditions. The following theorem provides the controller design conditions in terms of LMIs such that the exponential stability of the states to the equilibrium point is assured.

Theorem 1. *System (14) is exponentially stabilizable in the local region $\Omega = \{x | x^T P^{-1} x < \rho\}$, if for the given decay rate $\sigma > 0$, there exists matrices $S = S^T$ and M_i such that*

$$S > 0, \tag{20}$$

$$\overline{\Gamma}_{ii} < 0, \tag{21}$$

$$\overline{\Gamma}_{ij} + \overline{\Gamma}_{ji} < 0, \tag{22}$$

$$\begin{bmatrix}\left(\frac{u_{\lim}}{\varepsilon}\right)^2 & M_i^{(k)}\\ M_i^{T^{(k)}} & \rho S\end{bmatrix} > 0, \tag{23}$$

where

$$\overline{\Gamma}_{ij} = \begin{bmatrix}\left\{SA_i^T + A_i S + \frac{1+\varepsilon}{2}M_j^T B_i^T + \frac{1+\varepsilon}{2}B_i M_j + \sigma S\right\} & B_i^T & \left(\frac{1-\varepsilon}{2}\right)M_j^T\\ B_i & -\tau I & 0\\ \left(\frac{1-\varepsilon}{2}\right)M_j & 0 & -\tau^{-1}I\end{bmatrix}. \tag{24}$$

Proof. Consider the exponential Lyapunov stability conditions with the decay rate σ, as

$$\dot{V} + \sigma V < 0, \tag{25}$$

where the Lyapunov candidate is chosen as

$$V = x^T(t)Px(t), \tag{26}$$

where P is a symmetric positive definite matrix. Substituting (14) into (25), the exponential stability condition is continued as

$$V = x^T(t)\left\{\sum_{i=1}^{128}\sum_{j=1}^{128}\rho_i(\theta)\rho_j(\theta)\left\{A_i + \frac{1+\varepsilon}{2}B_iF_j\right\}^T P + P\left\{A_i + \frac{1+\varepsilon}{2}B_iF_j\right\} + \sigma P\right\}x(t)$$
$$+ r^T(t)\sum_{i=1}^{128}\rho_i(\theta)B_i^T P x(t) + x^T(t)P\sum_{i=1}^{128}\rho_i(\theta)B_i r(t) \tag{27}$$
$$= \sum_{i=1}^{128}\sum_{j=1}^{128}\rho_i(\theta)\rho_j(\theta)\begin{bmatrix} x^T(t) & r^T(t)\end{bmatrix}Q_{ij}\begin{bmatrix} x(t) \\ r(t)\end{bmatrix},$$

where

$$Q_{ij} = \begin{bmatrix} \left(A_i + \frac{1+\varepsilon}{2}B_iF_j\right)^T P + P\left(A_i + \frac{1+\varepsilon}{2}B_iF_j\right) + \sigma P & B_i^T P \\ PB_i & 0\end{bmatrix}. \tag{28}$$

Applying Lemma 2 on (27) subject to (15) results in

$$\sum_{i=1}^{128}\sum_{j=1}^{128}\rho_i(\theta)\rho_j(\theta)\begin{bmatrix} x^T(t) & r^T(t)\end{bmatrix}\overline{Q}_{ij}\begin{bmatrix} x(t) \\ r(t)\end{bmatrix}, \tag{29}$$

where

$$\overline{Q}_{ij} = \begin{bmatrix} \left\{\left(A_i + \frac{1+\varepsilon}{2}B_iF_j\right)^T P + P\left(A_i + \frac{1+\varepsilon}{2}B_iF_j\right)\right\} & B_i^T P \\ +\tau F_i^T F_i\left(\frac{1-\varepsilon}{2}\right)^2 + \sigma P & \\ PB_i & -\tau I\end{bmatrix}. \tag{30}$$

Applying Lemma 1 on (27) results in

$$\begin{cases} \overline{Q}_{ii} < 0, & \text{for } i = 1, \ldots, 128, \\ \overline{Q}_{ij} + \overline{Q}_{ji} < 0, & \text{for } i < j \text{ and } j = 1, \ldots, 128.\end{cases} \tag{31}$$

Considering the Schur complement, (31) leads to

$$\begin{cases} \Gamma_{ii} < 0 & \text{for } i = 1, \ldots, 128, \\ \Gamma_{ij} + \Gamma_{ji} < 0 & \text{for } i < j \text{ and } j = 1, \ldots, 128,\end{cases} \tag{32}$$

where

$$\Gamma_{ij} = \begin{bmatrix} \left\{\left(A_i + \frac{1+\varepsilon}{2}B_iF_j\right)^T P + \right. & B_i^T P & \left(\frac{1-\varepsilon}{2}\right)F_i^T \\ \left. P\left(A_i + \frac{1+\varepsilon}{2}B_iF_j\right) + \sigma P\right\} & & \\ PB_i & -\tau I & 0 \\ \left(\frac{1-\varepsilon}{2}\right)F_i & 0 & -\tau^{-1}I\end{bmatrix}. \tag{33}$$

Pre- and postmultiplying (32) by $\mathrm{diag}(P^{-1}, I, I)$ and defining the LMI variables $S = P^{-1}$ and $M_i = F_iP^{-1}$ result in (21) and (22). Moreover, the constraint $P = P^T > 0$ leads to the LMI (20). On the other hand, (15) holds in the local region $\Omega_1 = \{x||u| < (1/\varepsilon)\}$. Consequently, inspired from the set inverse analysis [41] and considering the same procedure discussed in [42], the condition which guarantees the ellipsoid $\Omega = \{x|x^TPx < \rho\}$ being inside the domain Ω_1, i.e., $\Omega \subset \Omega_1$, is given by

$$F_i^{(k)}\left(\frac{P}{\rho}\right)^{-1}F_i^{T(k)} < \left(\frac{1}{\varepsilon}\right)^2, \quad \text{for } i = 1, \ldots, r, \tag{34}$$

where F_i^k indicates the k-th row of F_i. By employing the Schur complement on condition (34), LMI (23) is obtained. The proof is completed.

In most of the existing results on the primary control of power components connected to a microgrid, the control law for each power electronic converters is constructed based on the states of its corresponding component [21–23]. This reduces the complexity of designing the control signal. However, the closed-loop stability overall MG is not guaranteed, as the

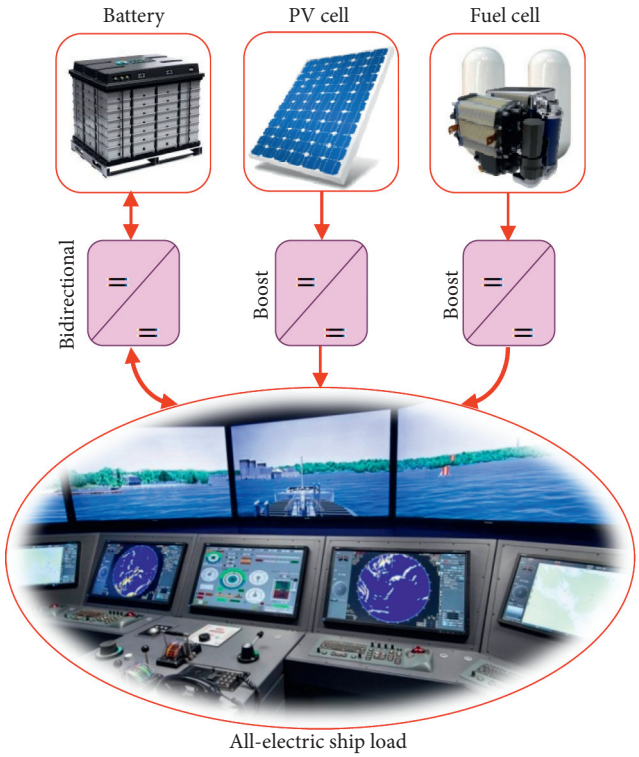

Figure 1: The considered power resources to supply 10 kw load.

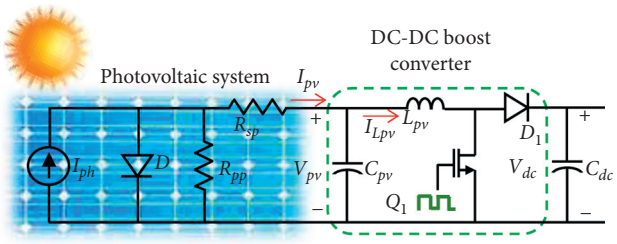

Figure 2: The photovoltaic (PV) array and its interface circuit used in the system.

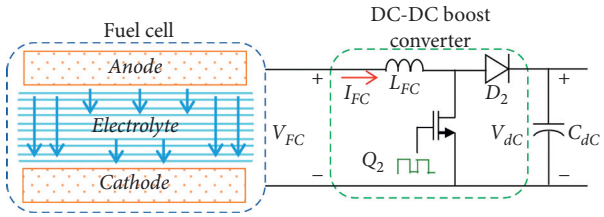

Figure 3: The fuel cell package and boost converter used in the system.

interconnections and effects of other components are not involved. Here, in this paper, a centralized controller is considered in which all available information of all components is used to design control signals. This consideration assures the closed-loop stability with the expense of increasing the complexity of the design procedure. In other words, as can be seen in (7), the

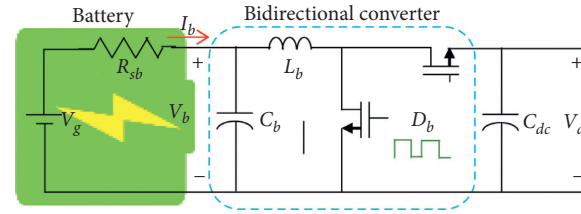

Figure 4: The energy storage and its interface circuit used in the system.

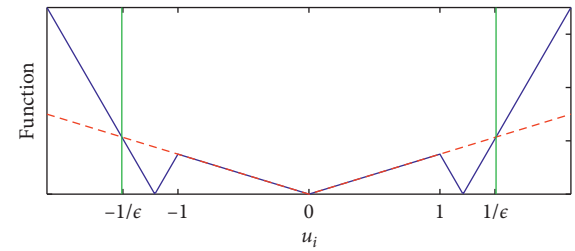

Figure 5: The functions of Lemma 1 (the $|r(t)|$ by the solid blue line and the $(1-\varepsilon/2)|u(t)|$ by the dashed red line).

overall system state vector comprises 7 state variables, and the dynamics have 3 nonlinearities and 4 time-varying parameters. Assuring stability for such a system is not a trivial task. Among the nonlinear control techniques, the LPV-based control approach uses linear control and convexity theories to design a stabilizing controller based on a systematic numerical procedure. This feature makes the LPV-based control method suitable for highly nonlinear and high-dimensional systems.

Generally, constraints (20)–(23) are matrix inequalities and contain several unknown variables to be found. Thereby, it is not possible to solve them analytically. This issue persuades using the LMI solver. The way of designing a nonlinear gain-scheduling controller for system (7) is provided in Figure 6. For a given dynamical nonlinear system with physical bounds of nonlinear and time-varying parameters, the equivalent polytopic-LPV representation can be obtained systematically based on the sector-nonlinearity modeling approach [35].

Then, the scheduling parameter and local linear system matrices are achieved. The local linear system matrices are then utilized in Theorem 1 to numerically compute the controller gains via the LMI technique. Both unknown controller gains and Lyapunov matrices are calculated so that the constraints in Theorem 1 satisfy. Based on the proof of Theorem 1, the satisfaction of the constraints assures closed-loop stability theoretically. Finally, the LPV controller is constructed based on the scheduling parameters and calculated gains. All steps of controller design are done offline. The proposed controller is designed offline and does not expose an online computational burden, which is the main drawback of the model predictive controller [43, 44]. On the other hand,

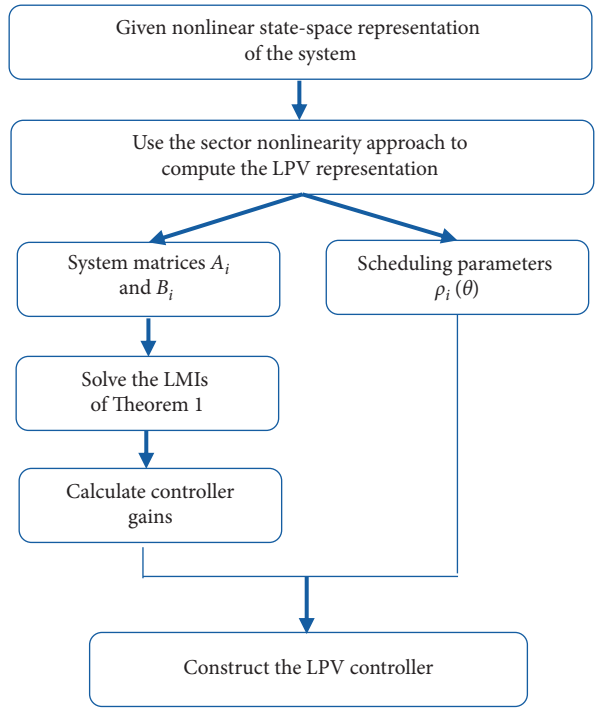

Figure 6: The LPV controller design procedure.

the linear proportional-integral-derivative (PID) controller [32] and linear quadratic regulator [33, 45] only assure the local stability around the operating point. However, the suggested LPV controller assures the stability of the system on the basis of its physical bounds of the nonlinear and time-varying parameters [46].

4. Real-Time Simulation Results and Discussion

In this section, the designed controller based on Theorem 1 is applied to the propulsion system of the EB dynamics (7). In order to reduce the controller design time burden and controller implementation, in Theorem 1, it is considered that $M_i = M$. Also, the nominal powers of the solar power plant, fuel cell, and energy storage are set as 5 kW, 5 kW, and 2 kW, respectively. To show the applicability of the suggested approach, a model-in-the-loop (MiL) real-time simulation is carried out as shown in Figure 7, where the dSPACE 1202 board is deployed for the rapid prototyping solution.

In the simulations, it is assumed that the solar irradiation is constant, and so, the solar cell voltage to extract the maximum power is fixed. To show the merits of the suggested control approach (Prop.), it is compared with the sliding mode control (SMC) [47] and adaptive backstepping control (ABP) [48]. Additionally, it is shown in [47] that the SMC approach outperforms the conventional proportional-integral (PI) controller. It should be noted that the DC MG structure considered in [47] is different from this paper. However, the SMC design procedure is modified by [48], which is used for the comparison. Moreover, the control approaches [47, 48] do not consider the issue of input saturation in their design procedures.

The closed-loop system is simulated in MATLAB software and the states and the averaged control inputs are shown in Figures 8 and 9.

Also, to quantitatively compare the results of the controllers, the norms 2 of the tracking errors of the voltages V_{DC}, V_B, and V_{PV} for these controllers are given in Table 1. As can be seen in Table 1, the proposed approach results in a smaller norm 2 for all voltages. Thereby, the tracking error based on the proposed approach outperforms the other approaches, since the proposed approach develops exponential stability and convergence in comparison with the asymptotic stability in the ABP and SMC.

As can be seen in Figure 8, the proposed approach exponentially stabilizes the nonlinear system. Additionally, from Figure 9, one infers that the control laws [47, 48] experience high oscillations for the early stage of the simulation. One of the reasons is that in those approaches, the input saturation is not involved in the design procedure. For the case study of this paper, although the ABP and SMC controllers regulate the closed-loop system with the input saturation, the transient performance is degraded. Further, by changing the initial conditions and changing the operating point, they may not stabilize the overall system.

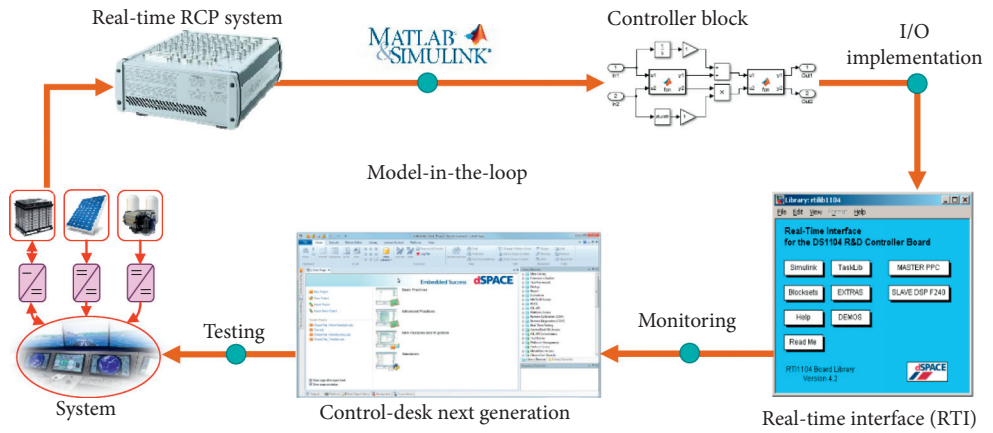

Figure 7: MiL real-time setup and configuration of the marine DC MG benchmark.

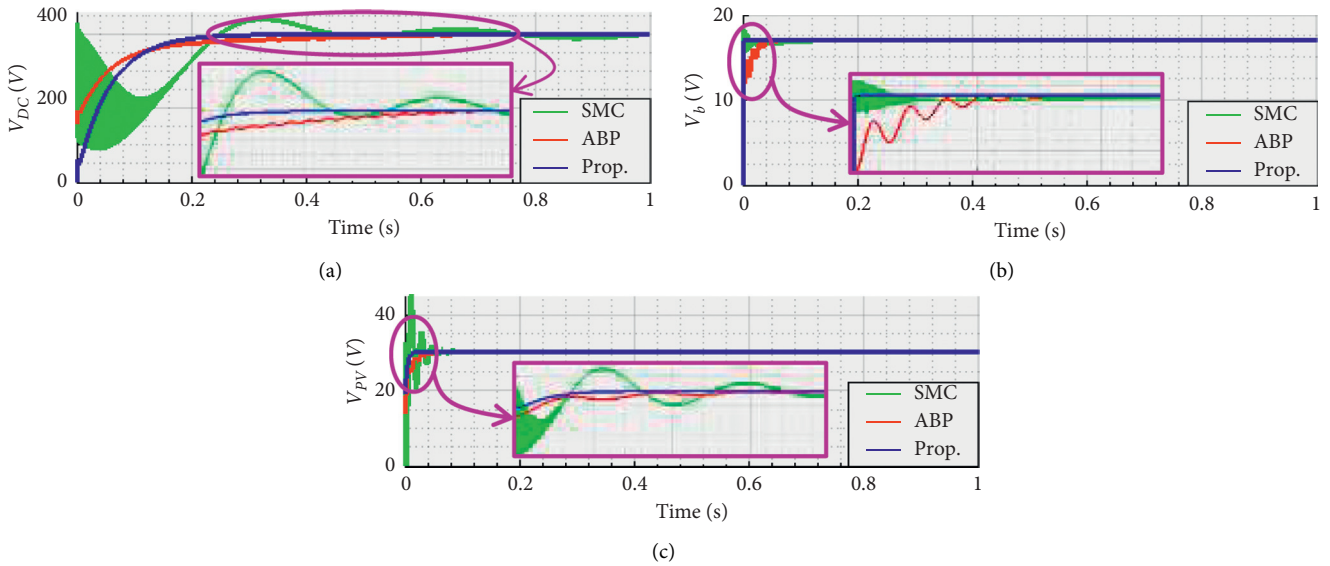

Figure 8: The voltages of the DC MG EB system. (a) DC-link, (b) battery, and (c) solar power plant.

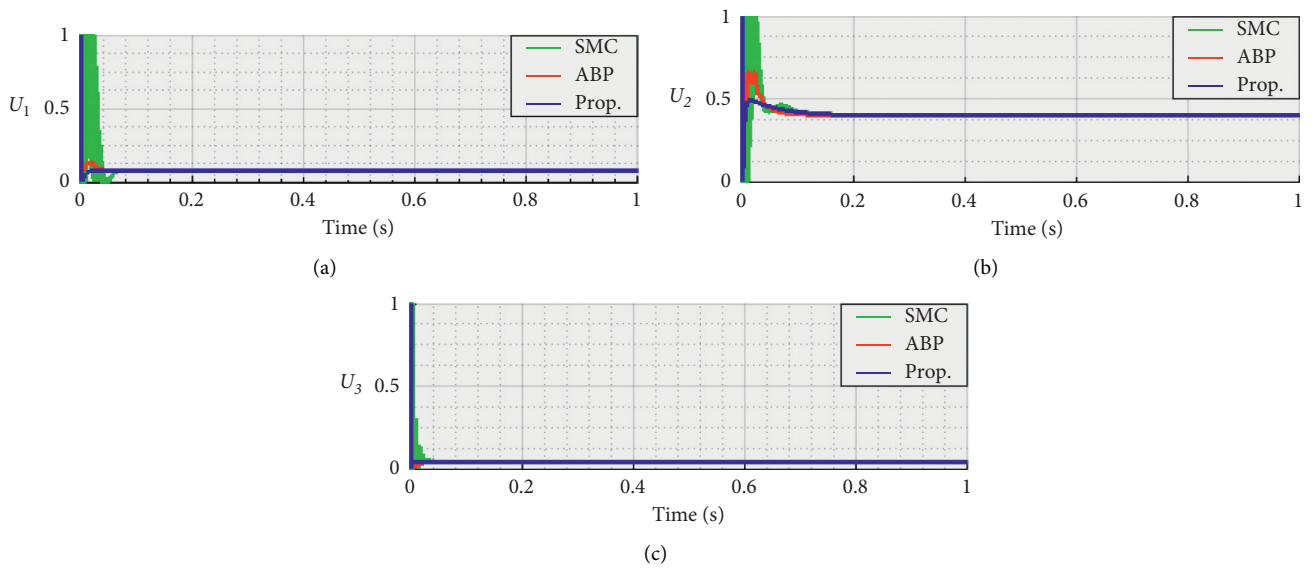

Figure 9: The control inputs of the DC MG EB system converters. (a) Solar plant, (b) fuel cell, and (c) battery.

Table 1: Norms 2 of the considered controller approaches.

	Prop.	ABP	SMC
V_{DC}	6.48911×10^4	8.3269×10^4	1.6737×10^5
V_B	77.6278	150.1197	558.4585
V_{PV}	582.5191	2.2616×10^3	1.0392×10^3

5. Conclusion

In this paper, the problem of the propulsion power system regulating the electric boat was investigated. A robust controller strategy was developed to optimally utilize the energy resources available in the DC power system. A nonlinear power system with a 5 kW solar power plant, 5 kW fuel cell, and 2 kW battery package is considered. By the means of the linear parameter varying (LPV) method, the suitable gains of the states' feedback controller are determined to provide the required PWM switching signals of the boost converters of the energy resources. The suggested control approach has a systematic offline design procedure based on the linear matrix inequality (LMI) technique. Therefore, it is a suitable approach for highly nonlinear and complex systems to assure closed-loop stability. The simulation results demonstrate the performance of the developed control method to effectively regulate the DC-link voltage fast and without fluctuations. For future work, considering nonlinear loads such as constant power loads (CPLs) and several fuel cells and batteries in the propulsion system to manage the power of the generators is suggested. Comparing the transient and steady-state of the suggested controller with other nonlinear approaches is recommended. Also, evaluating the effect of environmental changes, such as solar irradiation and faults, is a good research topic.

Data Availability

Data that support the findings of this study are available on request.

Conflicts of Interest

The authors declare that they have no conflicts of interest.

References

[1] C. M. Kang, S.-H. Lee, and C. C. Chung, "Discrete-time LPV observer with nonlinear bounded varying parameter and its application to the vehicle state observer," *IEEE Transactions on Industrial Electronics*, vol. 65, no. 11, pp. 8768–8777, 2018.

[2] M.-H. Khooban, M. Gheisarnejad, N. Vafamand, and J. Boudjadar, "Electric vehicle power propulsion system control based on time-varying fractional calculus: implementation and experimental results," *IEEE Transactions on Intelligent Vehicles*, vol. 4, no. 2, pp. 255–264, 2019.

[3] E. Alcala, V. Puig, J. Quevedo, and T. Escobet, "Gain-scheduling LPV control for autonomous vehicles including friction force estimation and compensation mechanism," *IET Control Theory & Applications*, vol. 12, no. 12, pp. 1683–1693, 2018.

[4] S. Yousefizadeh, J. D. Bendtsen, N. Vafamand, M. H. Khooban, T. Dragičević, and F. Blaabjerg, "EKF-based predictive stabilization of shipboard DC microgrids with uncertain time-varying loads," *IEEE Journal of Emerging and Selected Topics in Power Electronics*, vol. 7, no. 2, pp. 901–909, 2018.

[5] S. Chakraborty, H.-N. Vu, M. M. Hasan, D.-D. Tran, M. E. Baghdadi, and O. Hegazy, "DC-DC converter topologies for electric vehicles, plug-in hybrid electric vehicles and fast charging stations: state of the art and future trends," *Energies*, vol. 12, no. 8, p. 1569, 2019.

[6] Y. Cao, O. Kaiwartya, Y. Zhuang, N. Ahmad, Y. Sun, and J. Lloret, "A decentralized deadline-driven electric vehicle charging recommendation," *IEEE Systems Journal*, vol. 13, no. 3, pp. 3410–3421, 2019.

[7] X. Zhang, Y. Wang, G. Liu, and X. Yuan, "Robust regenerative charging control based on T–S fuzzy sliding-mode approach for advanced electric vehicle," *IEEE Transactions on Transportation Electrification*, vol. 2, no. 1, pp. 52–65, 2016.

[8] K. Mahmud, M. S. Rahman, J. Ravishankar, J. Hossain, and J. M. Guerrero, "Real-time load and ancillary support for a remote island power system using electric boats," *IEEE Transactions on Industrial Informatics*, vol. 16, no. 3, pp. 1516–1528, 2019.

[9] M. S. M. Sarif, T. X. Pei, and A. Z. Annuar, "Modeling, design and control of bidirectional DC-DC converter using state-space average model," in *Proceedings of the 2018 IEEE Symposium on Computer Applications & Industrial Electronics (ISCAIE)*, pp. 416–421, Penang, Malaysia, April 2018.

[10] J. Moreno-Valenzuela and O. García-Alarcón, "On control of a boost DC-DC power converter under constrained input," *Complexity*, vol. 2017, Article ID 4143901, 11 pages, 2017.

[11] J. Moreno-Valenzuela and J. Guzman-Guemez, "Experimental evaluations of voltage regulators for a saturated boost DC-to-DC power converter," *Transactions of the Institute of Measurement and Control*, vol. 38, no. 3, pp. 327–337, 2016.

[12] M. H. Khooban, N. Vafamand, and J. Boudjadar, "Tracking control for hydrogen fuel cell systems in zero-emission ferry ships," *Complexity*, vol. 2019, Article ID 5358316, 9 pages, 2019.

[13] K. Xiangli, S. Li, and K. M. Smedley, "Decoupled PWM plus phase-shift control for a dual-half-bridge bidirectional DC-DC converter," *IEEE Transactions on Power Electronics*, vol. 33, no. 8, pp. 7203–7213, 2018.

[14] X. Li, X. Ruan, X. Xiong, M. Sha, and C. K. Tse, "Approximate discrete-time small-signal models of DC-DC converters with consideration of practical pulsewidth modulation and stability improvement methods," *IEEE Transactions on Power Electronics*, vol. 34, no. 5, pp. 4920–4936, 2019.

[15] Z. Fang, H. Tian, and P. Li, "Probabilistic robust linear parameter-varying control of a small helicopter using iterative scenario approach," *IEEE/CAA Journal of Automatica Sinica*, vol. 2, no. 1, pp. 85–93, 2015.

[16] A. Hanif, A. I. Bhatti, and Q. Ahmed, "Managing thermally derated torque of an electrified powertrain through LPV control," *IEEE/ASME Transactions on Mechatronics*, vol. 23, no. 1, pp. 364–376, 2018.

[17] N. Aouani, S. Salhi, G. Garcia, and M. Ksouri, "New Robust stability and stabilizability conditions for linear parameter

time varying polytopic systems," in *Proceedings of the 2009 3rd International Conference on Signals, Circuits and Systems (SCS)*, pp. 1–6, Medenine, Tunisia, November 2009.

[18] A. Morsi, H. S. Abbas, and A. M. Mohamed, "Wind turbine control based on a modified model predictive control scheme for linear parameter-varying systems," *IET Control Theory & Applications*, vol. 11, no. 17, pp. 3056–3068, 2017.

[19] F. A. Inthamoussou, F. D. Bianchi, H. De Battista, and R. J. Mantz, "LPV wind turbine control with anti-windup features covering the complete wind speed range," *IEEE Transactions on Energy Conversion*, vol. 29, no. 1, pp. 259–266, 2014.

[20] T. Dridi, N. Aouani, and A. Mami, "V/f controlled photovoltaic pumping system under LPV model," in *Proceedings of the 2017 International Conference on Control, Automation and Diagnosis (ICCAD)*, pp. 516–521, Hammamet, Tunisia, January 2017.

[21] M. Mohamed, Z. Malika, Z. Khalida, and C. Jawad, "Modeling and optimization of a grid connected photovoltaic energy conversion system based on advanced nonlinear control," in *Proceedings of the 2019 International Conference of Computer Science and Renewable Energies (ICCSRE)*, pp. 1–10, Agadir, Morocco, July 2019.

[22] S. Rahmani, S. Ktata, K. Yeferni, F. Doub, A. Hamadi, and K. Al-Haddad, "A nonlinear control of pmsg based variable speed wind energy generation system connected to the grid," in *Proceedings of the 2019 19th International Conference on Sciences and Techniques of Automatic Control and Computer Engineering (STA)*, pp. 449–454, Sousse, Tunisia, March 2019.

[23] F. Zhang, Y. Ma, T. Zhu, and H. Chen, "Nonlinear control of air-feed system for proton exchange membrane fuel cell with auxiliary power battery," *Journal of Renewable and Sustainable Energy*, vol. 11, Article ID 054302, 2019.

[24] D. I. Martinez, J. J. De Rubio, T. M. Vargas et al., "Stabilization of robots with a regulator containing the sigmoid mapping," *IEEE Access*, vol. 8, pp. 89479–89488, 2020.

[25] J. De Jesús Rubio, "Structure regulator for the perturbations attenuation in a quadrotor," *IEEE Access*, vol. 7, pp. 138244–138252, 2019.

[26] J. O. Escobedo-Alva, E. C. García-Estrada, L. A. Páramo-Carranza, J. A. Meda-Campaña, and R. Tapia-Herrera, "Theoretical application of a hybrid observer on altitude tracking of quadrotor losing GPS signal," *IEEE Access*, vol. 6, pp. 76900–76908, 2018.

[27] J. D. J. Rubio, D. I. Martinez, V. Garcia et al., "The perturbations estimation in two gas plants," *IEEE Access*, vol. 8, pp. 83081–83091, 2020.

[28] C. Aguilar-Ibanez and M. S. Suarez-Castanon, "A trajectory planning based controller to regulate an uncertain 3D overhead crane system," *International Journal of Applied Mathematics and Computer Science*, vol. 29, no. 4, pp. 693–702, 2019.

[29] J. García-Sánchez, S. Tavera-Mosqueda, R. Silva-Ortigoza et al., "Robust switched tracking control for wheeled mobile robots considering the actuators and drivers," *Sensors*, vol. 18, no. 12, p. 4316, 2018.

[30] Y. M. Alsmadi, A. Alqahtani, R. Giral et al., "Sliding mode control of photovoltaic based power generation systems for microgrid applications," *International Journal of Control*, pp. 1–12, 2020.

[31] H. Armghan, M. Yang, M. Q. Wang, N. Ali, and A. Armghan, "Nonlinear integral backstepping based control of a DC microgrid with renewable generation and energy storage systems," *International Journal of Electrical Power & Energy Systems*, vol. 117, Article ID 105613, 2020.

[32] S. Zhuo, A. Gaillard, L. Xu, D. Paire, and F. Gao, "Extended state observer-based control of DC-DC converters for fuel cell application," *IEEE Transactions on Power Electronics*, vol. 35, no. 9, pp. 9923–9932, 2020.

[33] Q. Li and M. E. Baran, "A novel frequency support control method for PV plants using tracking LQR," *IEEE Transactions on Sustainable Energy*, vol. 11, no. 4, p. 2263, 2020.

[34] N. Vafamand, S. Yousefizadeh, M. H. Khooban, J. D. Bendtsen, and T. Dragicevic, "Adaptive TS fuzzy-based MPC for DC microgrids with dynamic CPLs: nonlinear power observer approach," *IEEE Systems Journal*, vol. 13, no. 3, pp. 3203–3210, 2018.

[35] N. Vafamand, A. Khayatian, and M. H. Khooban, "Stabilisation and transient performance improvement of DC MGs with CPLs: non-linear reset control approach," *IET Generation, Transmission & Distribution*, vol. 13, no. 14, pp. 3169–3176, 2019.

[36] N. Vafamand, M. H. Asemani, and A. Khayatian, "Robust," *IEEE Transactions on Fuzzy Systems*, vol. 26, no. 3, pp. 1401–1413, 2018.

[37] N. Vafamand and A. Khayatian, "Model predictive-based reset gain-scheduling dynamic control law for polytopic LPV systems," *ISA Transactions*, vol. 81, pp. 132–140, 2018.

[38] N. Vafamand, M. H. Asemani, and A. Khayatiyan, "A robust L1 controller design for continuous-time TS systems with persistent bounded disturbance and actuator saturation," *Engineering Applications of Artificial Intelligence*, vol. 56, pp. 212–221, 2016.

[39] C. Scherer and S. Weiland, *Linear Matrix Inequalities in Control*, Dutch Institute for Systems and Control, Delft, The Netherlands, 2004.

[40] N. Vafamand, S. Khorshidi, and A. Khayatian, "Secure communication for non-ideal channel via robust TS fuzzy observer-based hyperchaotic synchronization," *Chaos Solitons Fractals*, vol. 112, pp. 116–124, 2018.

[41] Y.-Y. Cao and Z. Lin, "Robust stability analysis and fuzzy-scheduling control for nonlinear systems subject to actuator saturation," *IEEE Transactions on Fuzzy Systems*, vol. 11, no. 1, pp. 57–67, 2003.

[42] D. Haiping D and N. Zhang, "Fuzzy control for nonlinear uncertain electrohydraulic active suspensions with input constraint," *IEEE Transactions on Fuzzy Systems*, vol. 17, no. 2, pp. 343–356, 2009.

[43] N. Vafamand, M. H. Khooban, T. Dragicevic, and F. Blaabjerg, "Networked fuzzy predictive control of power buffers for dynamic stabilization of DC microgrids," *IEEE Transactions on Industrial Electronics*, vol. 66, no. 2, pp. 1365–1362, 2018.

[44] Y. Shan, J. Hu, K. W. Chan, Q. Fu, and J. M. Guerrero, "Model predictive control of bidirectional DC-DC converters and AC/DC interlinking converters-A new control method for PV-wind-battery microgrids," *IEEE Transactions on Sustainable Energy*, vol. 10, no. 4, pp. 1823–1833, 2019.

[45] S. Sen and V. Kumar, "Decentralized output-feedback-based robust LQR V-f controller for PV-battery microgrid including generation uncertainties," *IEEE Systems Journal*, vol. 14, no. 3, pp. 4418–4429, 2020.

[46] Q. Xu, N. Vafamand, L. Chen, T. Dragičević, L. Xie, and F. Blaabjerg, "Review on advanced control technologies for bidirectional DC/DC converters in DC microgrids," *IEEE Journal of Emerging and Selected Topics in Power Electronics*, 2020, In press.

[47] A. Agarwal, K. Deekshitha, S. Singh, and D. Fulwani, "Sliding mode control of a bidirectional DC/DC converter with constant power load," in *Proceedings of the IEEE First International Conference on DC Microgrids (ICDCM)*, pp. 287–292, Atlanta, GA, USA, June 2015.

[48] T. K. Roy, M. A. Mahmud, A. M. T. Oo, M. E. Haque, K. M. Muttaqi, and N. Mendis, "Nonlinear adaptive backstepping controller design for islanded DC microgrids," *IEEE Transactions on Industry Applications*, vol. 54, no. 3, pp. 2857–2873, 2015.